Scientia Iranica B (2014) 21(4), 1424–1439

SCIENTIA IRANICA

Sharif University of Technology
Scientia Iranica
Transactions B: Mechanical Engineering
www.scientiairanica.com

Simulation and experimental investigation of performance and emissions of a turbocharged lean-burn natural gas engine considering thermal boundary layer

Sh. Kharazmi*, A. Mozafari and A. Hajilouy-Benisi

Department of Mechanical Engineering, Sharif University of Technology, Tehran, P.O. Box 11155-9567, Iran.

Received 18 February 2013; received in revised form 5 September 2013; accepted 4 December 2013

KEYWORDS
Natural gas;
Turbocharged;
Turbulence and combustion simulation;
Thermal boundary layer;
NO_x;
CO;
UHC;
CO_2.

Abstract. Emission characteristics of pure natural gas is fairly known, however more experimental investigation of natural gas combustion is necessary. In this research, emission and performance of a turbocharged natural gas SI engine are investigated experimentally at WOT and lean burn conditions. A computer code is also developed in MATLAB environment for predicting engine performance and NO emission and the results are validated with experimental data. Thermal boundary layer, as a novel approach, is considered in the simulation and a better agreement of predicted mass fraction burned was achieved at end part of combustion process when compared with experimental results. Experimental results have revealed that turbocharger match at mid engine speed, waste-gate opening and increase of friction losses at high engine speed resulted in better torque back-up. Boost pressure, controlled by compressor outlet pressure, remained nearly constant at speeds higher than 1450 rpm. NO emission reduced with engine speed increase due to shorter time that burned gases remain at high temperatures, although they have higher temperature at higher speeds. It however increased with the increase of excess air ratio until it reached to its peak value at about 1.1 from stoichiometric mixture and then decreased, while it decreased substantially with increase of spark timing retard. Brake specific UHC and CO_2 emissions were min at mid speed range and WOT.

1. Introduction

Fossil fuel consumption is steadily increasing as a result of population growth and improvements of living standard demand. World total energy consumption has grown by about 36% over the past 15 years. Internal combustion engine fuel resources depend on availability of fossil fuel supplies. Strict emission regulations are another issue facing the current generation of IC engines [1].

One of the favorite alternative fuels is natural gas. It is composed of methane with molar H/C ratio of 3.8 comparing with ratios of 1.8-2.0 for gasoline and diesel fuels. This higher ratio reduces CO_2 emission and so its greenhouse effects. 1 g methane produces 0.056 g CO_2/kJ while 1 g of gasoline and diesel produces 0.068 g CO_2/kJ and 0.071 g CO_2/kJ respectively. CO_2 emission of natural gas engine is about 20% lower than that of gasoline engine at the same power [2]. Natural gas produces lower CO and THC emissions. Higher RON of natural gas allows higher compression ratio thus producing higher thermal efficiencies. It also has relatively wider flammability limits, with better combustion in lean-burn strategies. Natural gas gives lower engine volumetric efficiency due

*. *Corresponding author. Tel: +98 21 66165667*
E-mail addresses: kharazmi@mech.sharif.edu (Sh. Kharazmi); mozafari@sharif.edu (A. Mozafari); hajilouy@sharif.edu (A. Hajilouy-Benisi)

to its injection in the intake manifold (compared to diesel fuel) and its lower stoichiometric fuel/air ratio (compared to gasoline) thus provides less power output. CNG DI engines have good volumetric efficiencies, but they have problematic load control and difficulties in injection control and technology and durability test. Turbocharger can offset this power reduction. It uses exhaust gas energy to compress intake air; therefore more fuel per displacement volume can be burned in a cycle. Turbocharging of SI engines has been improved less than diesel engines due to many difficulties, like knock phenomena and turbocharger matching with throttle valve [3].

Natural gas has significantly larger proven reserves compared with crude oil. The current known Reserves-to-Production (R/P) ratio for crude oil is about 40 years, while for natural gas it is about 60 years [1].

Emission standards are expected to become stricter in future. The European Automotive Manufacturers Association has determined 130 g/km CO_2 emission target for 2012 to 2015, with an additional 10 g/km CO_2 emission reduction coming from "complementary measures" including a greater use of biofuels. 65 percent of new cars will have to comply with the emission requirements in 2012, 75 percent in 2013, 80 percent in 2014 and 100 percent in 2015 [4]. NO_x emission has been the strictest Euro emission standard, with a limit of 0.4 g/(kWhr) in Euro VI. Table 1 shows standard values of emissions in recent years.

Cho and He [2] reviewed SI natural gas engines. Engine operating map, fuel economy, emissions, cycle-to-cycle variations in IMEP and strategies to achieve stable combustion of lean burn natural gas engines were highlighted. Stoichiometric natural gas engines were also briefly reviewed. They concluded that high activity catalyst for methane oxidation and lean de-NO_x system or three-way catalyst with precise air-fuel ratio control strategies should be developed to meet stringent emission standards.

Rothlisberger and Favrat [6] investigated the operation of a cogeneration natural gas engine with prechamber. They presented the limit of conventional lean burn operating mode with spark ignition (without prechamber) and discussed the prechamber geometrical configuration. They illustrated the influence of piston geometry and concluded that in comparison with the spark ignition (without prechamber), the prechamber ignition strongly intensified and accelerated the combustion process.

Table 1. The European emission standards, g/kWh [5].

Year	Standard	CO	HC	NO_x	PM
1992	Euro I	4.5	1.1	8.0	0.36
1996	Euro II	4	1.1	7	0.15
2000	Euro III	2.1	0.66	5	0.1
2005	Euro IV	1.5	0.46	3.5	0.02
2008	Euro V	1.5	0.46	2	0.02
2013	Euro VI	1.5	0.13	0.4	0.01

In another research [7], they studied the influences of spark timing, turbocharger specifications and engine load on prechamber ignition operation. They also presented a comparison between spark (without prechamber) and prechamber ignition. It was found that at rated power output, the prechamber ignition operation fulfilled the Swiss requirement for emission and achieved fuel conversion efficiency higher than 36.5%.

We have also studied turbocharged aftercooled gasoline engines by simulation and experiment [8]. We applied quasi-dimensional simulation on the engine and validated it with experiment results. We also found that intercooler fan had considerable effects on the turbocharged aftercooled engine performance at medium and high engine speeds at WOT and could be off at low loads and speeds.

Ghareghani et al. [9] investigated the thermal balance of a turbocharged, spark ignition engine fuelled by natural gas. Variation of output power, transferred energy to cooling fluid and exhaust gas energy at different operating conditions were compared experimentally. The maximum thermal efficiency of the turbocharged engine was 4% more than naturally aspirated at 2500 rpm. Also, the maximum thermal efficiency of the gas engine at 2500 rpm was 4.5% more than gasoline engine. Finally, based on experimental results, an empirical correlation was suggested to predict the energy of exhaust gases by using exhaust gas temperature and air fuel ratio.

Park et al. [10] investigated the applicability of a preexisting turbocharger designed for a CNG engine and correlated changes to the compression ratio with fuel economy, power, and torque levels of an HCNG engine. The potential benefits and the knocking characteristics of an HCNG engine with a higher compression ratio were assessed as considerations regarding its practical application in the field. Thermal efficiency was improved with the increase in compression ratio but adverse effects occurred and the excess air ratio that helps realize maximum thermal efficiency decreased from 1.8 to 1.6 for an HCNG engine due to a decrease in exhaust gas energy available for intake-air charging.

Use of stoichiometric air-fuel mixture with Exhaust Gas Recirculation (EGR) technique in a SI natural gas engine was experimentally investigated by Ibrahim and Bari [5]. Engine performance and NO emission were studied for both atmospheric and supercharged inlet conditions. It was found that the use of EGR had a significant effect on NO emissions.

Ibrahim and Bari [11] also compared the effects of both EGR and lean burn on natural gas SI engine performance at similar operating conditions. It was found that EGR dilution strategy was capable of producing extremely lower NO emission than lean burn technique. NO emission reduced by about 70% when the inlet charge was diluted at a rate of 20% using EGR instead of excess air.

Kesgin [12] studied the effects of design and operational parameters on the NO_x emissions of a turbocharged natural gas engine. A gas engine series used in combined power plants was optimized regarding power, efficiency and emissions. Since evaluation of the emission behavior has become increasingly important, the nitrogen oxide emission and its dependence on engine operational and geometrical conditions were investigated by using a zero-dimensional reaction kinetic model. The results showed improvement potential from emission point of view for developing new engines. They concluded that increase in engine speed, and also increase in excess air ratio caused a significant decrease in NO emissions. He also showed that charge temperature highly affected the level of NO emissions. In another paper [13], Kesgin predicted the effects of design and operating parameters on the NO_x emission of the same engine series, by genetic algorithm and artificial neural network. Kesgin also [14] investigated the effects of turbocharging system on the performance of the stationary engine. The effects of exhaust and turbocharging system parameters on the engine performance were predicted. Furthermore, he [15] investigated the inlet and exhaust system design of the stationary engine. Proper sizing of the inlet and exhaust pipe systems were precisely predicted.

Pourkhesalian et al. [16] performed a detailed comparison between some conventional and alternative fuels. Engine performance and exhaust emissions were experimentally studied for gasoline, methane and methanol in a wide range of engine operating conditions. For propane, ethanol and hydrogen, a thermodynamic model of SI engine was developed and validated. It was concluded that volumetric efficiency of the hydrogen engine was the lowest (28% less that gasoline engine), gasoline produce more power than the all other alternative fuels, and BSFC of methanol was 91% higher than that of gasoline while BSFC of hydrogen was 63% less than that of gasoline.

Korakianitis [1] extensively reviewed use of natural gas as a fuel in reciprocating CI and SI engines. Engine performance, combustion characteristics and emission levels were investigated.

There is more need for experimental and theoretical studies of natural gas combustion in internal combustion engines. For instance the turbulent flame speed, flame propagation characteristics, and emissions generation characteristics of pure natural gas in these engine operating conditions are not well known yet [1]. Here, a turbocharged pure natural gas SI engine is investigated experimentally. A thermodynamic simulation of the turbocharged pure natural gas SI engine in Matlab environment has also been developed and validated. Laminar flame speed of Witt and Griebel for CH_4 quoted by Lammle [17] is applied. Mean value modeling of Bargende also quoted by Lammle [17] has been used to calculate turbulence parameters during compression and combustion processes. Intake flow effects on Turbulent Kinetic Energy (TKE) have been taken as initial values. Compression, squish and dissipation effects on TKE have been considered in step by step calculations. Gulder equation [18] has been used to calculate turbulent flame speed from laminar flame speed. In this research, flame front area was calculated considering hemispherical flame front and its intersections with Mexican hat top of piston and cylinder walls. Thermal boundary layer was considered in combustion process to provide a better agreement for predicted mass fraction burned at the end part of combustion process when compared with experimental results. Thermodynamic properties of reactants and products including methane have precisely been obtained from correlations based on JANAF thermo-chemical tables [19]. Emission and performance characteristics of the engine have been presented and discussed.

2. Engine specifications and experimental setup

2.1. Engine specifications

The experimental engine was a Diesel-based turbocharged CNG engine. The main engine specifications are summarized in Table 2. The compression ratio of engine had been reduced from 16.82 to 10.5 through modification of piston bowl geometry in order to use CNG instead of diesel fuel. The engine had been equipped with new cylinder head, which enabled the fitting of spark plugs at the locations of diesel fuel injectors. The engine had been turbocharged at Sharif University turbocharging lab within the framework of a previous research and development project in cooperation with Sharif University and industry.

2.2. Experimental setup

The experimental investigation was carried out at the turbocharging lab of Sharif University of Technology (SUT); its schematic is shown in Figure 1. The test bed was equipped with an eddy current dynamometer with an accuracy of ± 1 Nm and ± 1 RPM. Ambient temperature, engine charge air temperature after intercooler, charge mixture temperature at inlet manifold, exhaust temperature before turbocharger turbine and inlet and outlet coolant temperatures were measured by

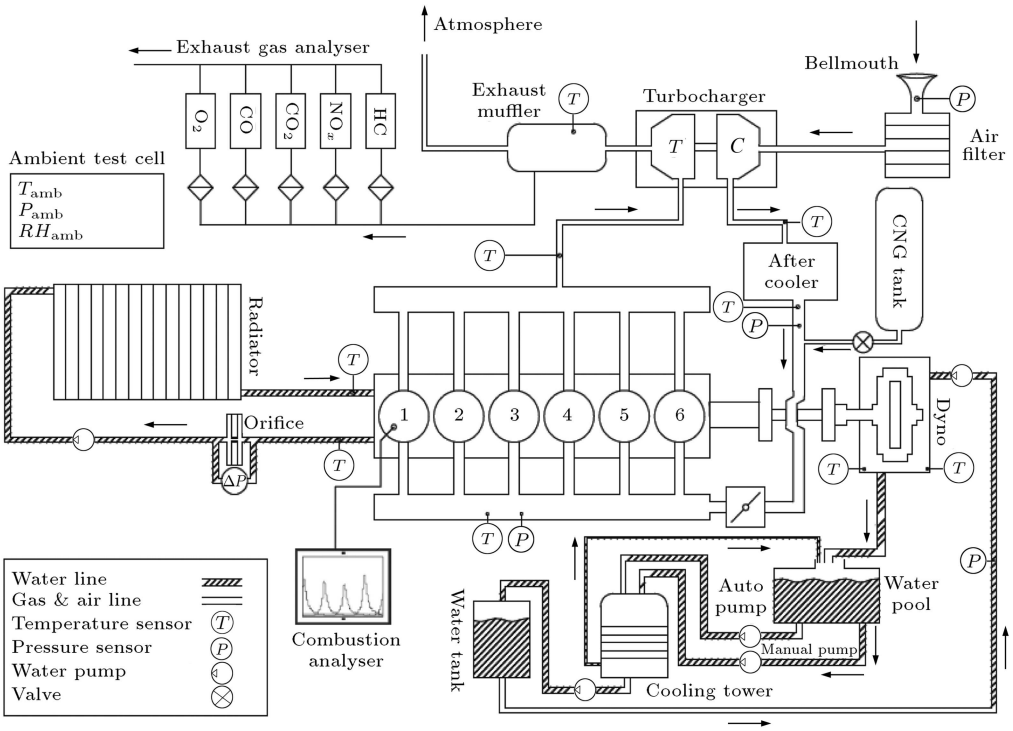

Figure 1. Schematic of turbocharging lab at Sharif University of Technology [20].

Table 2. The test engine main specifications.

No. and arrangement of cylinders	6 in line
Displacement volume	11.58 liter
Stroke	128 mm
Bore	150 mm
Connecting rod	280 mm
Compression ratio	10.5:1
Number of valves	2 inlets and 2 outlets
Turbocharger	Twin-entry waste-gated water-cooled CNG Schweitzer S300G
Firing order	1-5-3-6-2-4
Spark timing	25 °bTDC
λ_{mean}	1.25
Piston bowl vol.	184 cm^3
Piston bowl upper surface area	95 cm^2
Combustion chamber in cylinder head vol.	0 cm^3

J and K-type thermocouples calibrated within ±1 K. Ambient pressure was measured by a strain-gauge absolute pressure transducer calibrated with accuracy of ±136 Pa. Boost pressure was also measured with accuracy of ±136 Pa.

Since the engine was turbocharged, it was possible to use a bellmouth for engine air consumption measurement [21], with throat diameter of 3 inch (76.2 mm). Differential static pressure of the bellmouth throat and ambient was measured with an accuracy of ±10 Pa. The flow calculation equation is:

$$\dot{q}_{ac}\ (\mathrm{kg/s}) = 0.022\sqrt{\sigma \Delta P\ (\mathrm{mmH_2O})}, \quad (1)$$

where σ is ρ/ρ_s, i.e. ratio of air density at inlet of bellmouth to that of standard conditions [22].

AVL exhaust gas analyzer of DiCom 4000 was used to measure exhaust gas composition. Dry-basis volumetric (or mole) fraction of CO_2, CO, O_2, UHC and NO_x were measured in accordance with the United Nations Economic Commission for Europe (ECE) as well as excess air ratio [23]. The measuring range and accuracy is according to Table 3.

Spark timing was measured by AVL timing light. Engine cylinder pressure variation with crank angle was also measured by Kistler 6118B spark plug piezoelectric

Table 3. Technical parameters of AVL DiCom 4000 [23].

No.	Gas	Measuring range	Measuring accuracy
1	CO	0-10% by vol.	0.01% by vol.
2	CO_2	0-20% by vol.	0.1% by vol.
3	UHC	0-20 000 ppm by vol.	1 ppm by vol.
4	NO_x	0-5000 ppm by vol.	1 ppm by vol.
5	O_2	0-4% by vol.	0.01% by vol.
		4-22% by vol.	0.1% by vol.

pressure transducer, CA encoder 2614A and TDC sensor of 2629B. Experimental data were presented according to DIN 70020 standard.

All experiments were performed in steady state conditions at wide open throttle when the engine speed became steady within ±20 rpm, and exhaust temperature became to some extend constant.

3. Modeling

The engine simulation model is a quasi-dimensional two-zone model for describing dynamic behavior during the compression, combustion and expansion strokes. In this simulation, the combustion chamber is divided into two zones by flame front. The first zone contains unburned and the second one contains burned mixture. The flame front is assumed to travel by turbulent flame speed which is a function of laminar flame speed. The engine model uses Hohenberg correlation [24] to estimate engine heat losses. It is assumed that the flame propagates in a spherical like shape. The frictional losses in an internal combustion engine can be categorized into three main components: The rubbing friction, the pumping work and the accessory work. The simulation also includes Chen-Flynn friction model to predict friction mean effective pressure [25]. The composition of the reaction products is calculated from the chemical equilibrium of the 13 species at a given pressure and temperature. Finally, using Newton-Raphson method, molar fraction of each species as well as total mole fraction are calculated.

3.1. Turbulence simulation

Turbulence and combustion have twofold effects. Turbulence wrinkles flame front and increases its area in the combustion chamber. On the other hand specific volume of products is about four times that of reactants [26]. This rapid volume increase of the gases, passing through thin flame front in the limited volume of the combustion chamber, produces turbulence. In fact, turbulence intensifies combustion and also combustion increases the intensity of the turbulence.

Measurements at different points of combustion zone show that turbulence intensity is relatively homogeneous. In addition where there is no considerable swirl in intake flow, turbulence intensity is isotropic during the steps near TDC [26].

The turbulence model has been built up using mean values (averaged over the entire combustion chamber volume) and no differentiation between unburned and burned zones has been applied. Intake flow through intake port, which behaves like a jet flow, is the source of turbulence in the cylinder. Turbulent Kinetic Energy (TKE) at the time of Intake Valve Close (IVC) is assumed to be 20% of the intake flow mean velocity squared [17]. There are 3 terms in $k-\varepsilon$ equation which are related to TKE dissipation and TKE production due to compression and squish:

$$\frac{dk}{dt} = \left(\frac{dk_{\text{comp}}}{dt}\right) + \left(\frac{dk_{\text{squish}}}{dt}\right) - \left(\frac{dk_{\text{diss}}}{dt}\right). \quad (2)$$

Turbulent kinetic energy production due to compression is calculated by assuming mass and angular momentum conservation of eddy. Turbulent production due to squish is calculated from radial and axial components of in-cylinder flow velocity near TDC. Dissipation term is based on assuming that an eddy is dissipated after a few turns [17].

Turbulent kinetic energy is calculated step by step in each crank angle degree. Turbulence intensity is calculated from TKE. Integral length scale is obtained from mass conservation of eddy [17].

3.2. Laminar flame speed and EGR effects

There are a lot of flame speed data for CNG and methane, when mixed with other gases [27-34]. There are also some experiment-based relations for pure methane and CNG laminar flame speeds [17,26,35-38].

It is quoted by Lammle [17] that Witt and Griebel proposed methane laminar flame speed relation considering special turbocharged combustion conditions, i.e. higher unburned mixture temperature and cylinder pressure. Witt and Griebel relation is valid for unburned temperatures up to 850 K, while those of others like [35-37] are valid for up to 550 K and extended for up to 650 K at most [38]. Their laminar flame speed is in the following form for mixture of methane and air without EGR:

$$S_L = c.p_{\text{cyl}}^{-d}. \quad (3)$$

EGR effects on CNG laminar flame speed are considered by experimental relation proposed by Liao [36]. Therefore laminar flame speed for mixture of methane and air containing EGR takes the form:

$$S_L = c.p_{\text{cyl}}^{-d}(5.4825.rg_{\text{Vol}}^2 - 4.1988.rg_{\text{Vol}} + 0.9952). \quad (4)$$

In this relation, p_{cyl} is cylinder pressure, rg_{Vol} is total EGR volumetric fraction and c and d are parameters depending on T_u (unburned mixture temperature) and Φ (fuel air equivalence ratio) as:

For $p_{\text{cyl}} < 7$ bar:

$$\begin{aligned} c =& (-1.03 \times 10^{-2} T_u + 3.645).\Phi^2 \\ &+ (-4.12 \times 10^{-6} T_u^2 + 2.512 \times 10^{-2} T_u - 7.68).\Phi \\ &+ (8.78 \times 10^{-6} T_u^2 - 1.547 \times 10^{-2} T_u + 4.19), \quad (5) \end{aligned}$$

$$d = 7.5 \times 10^{-1}\Phi^2 - 1.6\Phi + 1.337 - 2 \times 10^{-4} T_u, \quad (6)$$

and for $p_{cyl} > 7$ bar:

$$c = (-6.906\times10^{-5}T_u^2 + 6.875\times10^{-2}T_u - 25.13).\Phi^3 + (1.155\times10^{-4}T_u^2 - 1.1523\times10^{-1}T_u + 46.47).\Phi^2 + (-4.185\times10^{-5}T_u^2 + 4.922\times10^{-2}T_u - 24.82).\Phi + (6.57\times10^{-6}T_u^2 - 9.55\times10^{-3}T_u + 5.185), \quad (7)$$

$$d = 0.45. \quad (8)$$

3.3. Turbulent flame speed

Gulder [39] studied turbulent combustion models and proposed the ratio of premixed turbulent flame speed to laminar flame speed for 3 different combustion regimes (wrinkled laminar-flame, flamelets-in-eddies regime, and distributed-reaction regime). He also used experimental flame speed results of methane by [38,39] for validation. Turbulent flame speed appropriate for engine combustion is in the wrinkled regime and is defined as:

$$\frac{S_T}{S_L} = 1 + 0.62\left(\frac{u'}{S_L}\right)^{1/2} \mathrm{Re}_T^{1/4}. \quad (9)$$

In Eq. (9), S_T and S_L are turbulent and laminar flame speeds, respectively. Re_T is the turbulent Reynolds number which is defined as:

$$\mathrm{Re}_T = \left(\frac{u' l_i \rho_U}{\mu}\right), \quad (10)$$

where u' is the turbulence intensity of the cylinder contents, ρ_U and μ are the unburned mixture density and dynamic viscosity, respectively, and l_i is the integral length scale.

3.4. Novel approach for the end part of combustion

When the flame approaches the cylinder walls, the turbulent length scales that can wrinkle the flame front reduce and consequently mass burning rate decreases. Proximity of flame to the cylinder walls also leads to higher heat losses and resulted in decrease of mass burning rate. Finally the flame extinguishes due to termination of reactants, low temperature of reactants and lack of chemical radicals at the proximity of the cylinder walls [40]. Keck [41] proposed an exponential decay for final mass burning rate. Therefore, it is clear that turbulent burning velocity by itself is insufficient to describe a turbulent flame in an engine [40]. Thus, in order to better simulate the end part of combustion in this research, a thermal boundary layer has been considered during the combustion process. There are few references about the cylinder thermal boundary layer. Lyford-Pike and Heywood [42] measured the thickness of thermal boundary layer in an IC engine. This measurement was done by Schlieren approach on different sections of combustion chamber, i.e. cylinder liner, cylinder head, and piston during complete operating cycle. Taking the idea of thermal boundary layer from [42], it has been assumed in this research that thermal boundary layer thickness is equal to quench layer. The temperature of thermal boundary layer is low due to heat losses to cylinder walls, and its thickness is calculated from mass fraction burned curves. This thickness should be equal to a value that if be subtracted from cylinder dimensions adjacent to its walls, total mass fraction burned at the end of combustion is equal to corresponding experimental value.

3.5. Assumptions

1. Cylinder content is considered to be homogeneous during compression and expansion processes.
2. Two-zone combustion model is used. Each zone is assumed to be homogeneous.
3. It is assumed that all gases are ideal.
4. Effects of blow-by and crevices are ignored.
5. The flame front thickness is assumed to be negligible.
6. Cylinder wall temperature is assumed to be constant.
7. Combustion chamber wall surfaces in contact with burned and unburned zones are calculated by considering a hemispherical flame progress with center at spark plug.
8. Engine is running at steady state conditions.
9. Cylinder pressure at the end of each calculating step is assumed to be uniform through the whole cylinder.
10. Heat transfer between burned and unburned zones is neglected; however each zone has heat losses with the cylinder walls.
11. Thirteen species (CO_2, CO, H_2O, H_2, O_2, N_2, O, H, OH, N, NO, NO_2 and unburned fuel as CH_4) are considered to be combustion products and in chemical equilibrium during combustion and expansion processes.
12. The effects of EGR are considered in theoretical validation calculations.
13. Turbulence is assumed to be homogeneous and isotropic.
14. Intake manifold temperature and static pressure of experimental results are assumed for mixture at the first step of compression.
15. Every degree of crank revolution is considered as one step in theoretical calculations.

3.6. NO formation kinetic model

The extended Zeldovich mechanism [26] is applied to determine the rate of change of NO concentration during combustion and expansion processes as:

$$\frac{d[\mathrm{NO}]}{dt} = \frac{2R_1\{1-([\mathrm{NO}]/[\mathrm{NO}]_e)^2\}}{1+([\mathrm{NO}]/[\mathrm{NO}]_e)R_1/(R_2+R_3)}, \tag{11}$$

where:

$$R_1 = k_1^+[\mathrm{N_2}]_e[\mathrm{O}]_e = k_1^-[\mathrm{NO}]_e[\mathrm{N}]_e, \tag{12}$$

$$R_2 = k_2^+[\mathrm{N}]_e[\mathrm{O_2}]_e = k_2^-[\mathrm{NO}]_e[\mathrm{O}]_e, \tag{13}$$

$$R_3 = k_3^+[\mathrm{N}]_e[\mathrm{OH}]_e = k_3^-[\mathrm{NO}]_e[\mathrm{H}]_e, \tag{14}$$

for the principal reactions, respectively, given as:

$$\mathrm{N_2 + O} \underset{k_1^-}{\overset{k_1^+}{\leftrightarrow}} \mathrm{NO + N}, \tag{15}$$

$$\mathrm{N + O_2} \underset{k_2^-}{\overset{k_2^+}{\leftrightarrow}} \mathrm{NO + O}, \tag{16}$$

$$\mathrm{N + OH} \underset{k_3^-}{\overset{k_3^+}{\leftrightarrow}} \mathrm{NO + H}, \tag{17}$$

where [ ] denotes the concentration, and the subscript e refers to the equilibrium value. The rate constants k are in units of $\mathrm{m^3/kmol/s}$ and have been calculated from GRI-MECH 3.0 [43].

3.7. Theoretical calculations

Calculations are carried out step by step with every degree of crank revolution as one step. Heat losses from cylinder contents to its surrounding surfaces is calculated by the Hohenberg semi-empirical relation [24], the most appropriate relation for CNG engines [44]. Hence, the first law of thermodynamic is satisfied for each step. A hemispherical flame front propagates from spark plug located at the center of combustion chamber cylinder head. When this hemisphere radius is less than l_i, turbulence does not wrinkle the flame. As the flame radius increases, the effect of turbulence becomes more important. It is assumed that when the flame radius reaches l_i, turbulent flame propagation is established and its speed is calculated according to Eq. (9). Two-zone combustion model is used to simulate combustion process. Flame front propagation and intersection with Mexican-hat bowl of piston and cylinder liner are precisely calculated based on cylinder geometry. Initial pressure and temperature of mixture is estimated from experimental results.

3.8. Thermal Boundary Layer (TBL) effects

In order to show the effects of thermal boundary Layer, two different predicted mass fraction burned and corresponding cylinder pressure for two different operating conditions have been presented and compared with experimental results of [17] in Figures 2 to 5. Considering thermal boundary layer in combustion simulation resulted in negligible deviation between simulation and experiment curves of the mass fraction burned at end part of combustion as seen in Figures 2 and 4. Considering thermal boundary layer also resulted in well simulation of combustion duration in CAo. Cylinder pressure was also simulated well, shown in Figures 3 and 5.

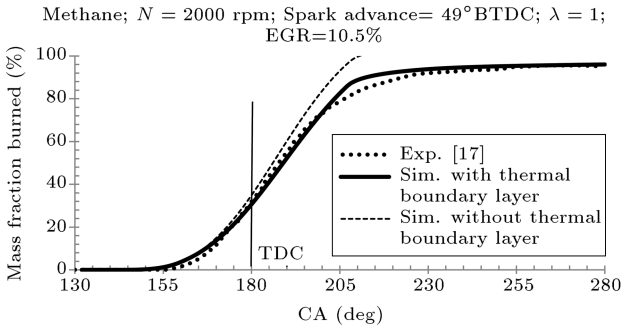

Figure 2. Comparison of simulation, with and without consideration of thermal boundary layer, with experiment for mass fraction burned.

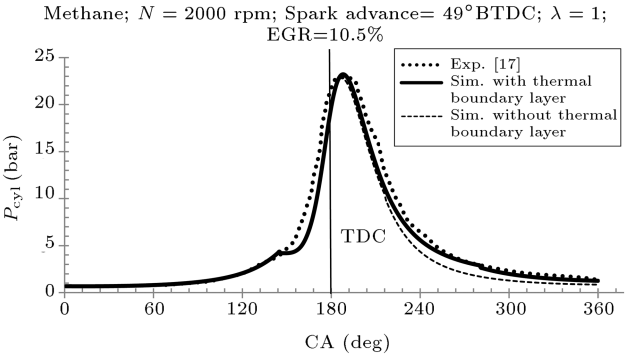

Figure 3. Comparison of simulation, with and without consideration of thermal boundary layer, with experiment for cylinder pressure.

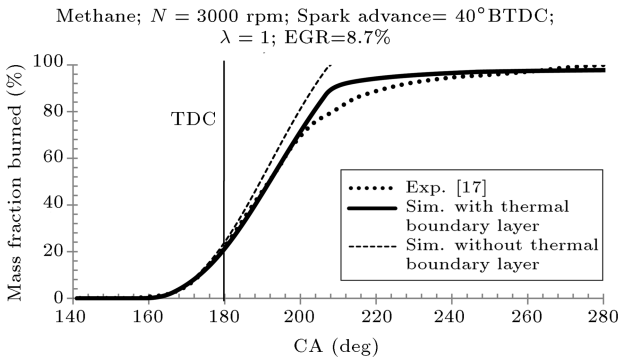

Figure 4. Comparison of simulation, with and without consideration of thermal boundary layer, with experiment for mass fraction burned.

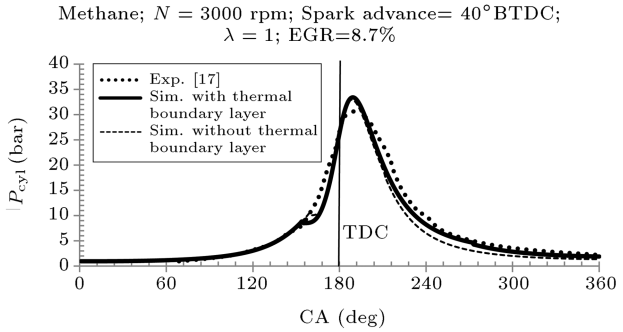

Figure 5. Comparison of simulation, with and without consideration of thermal boundary layer, with experiment for cylinder pressure.

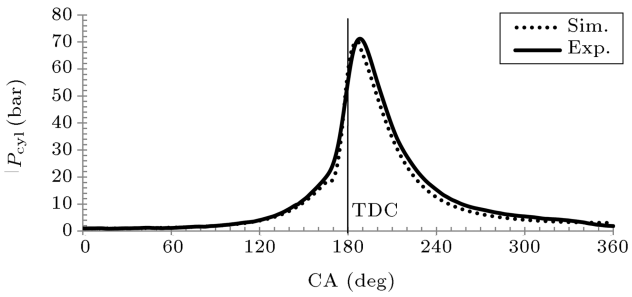

Figure 6. Experimental and simulated cylinder pressure variation with crank angle at 800 rpm, part load, spark timing of 25° bTDC and λ_{mean} of 1.25.

4. Model validation, parametric study, test results and discussions

It is necessary to study diesel-based NG engine performance and emissions by simulation and experimental investigations. Emission generation characteristics of pure natural gas is not especially well-known, hence experimental investigation of NG combustion is necessary.

4.1. Model validation

Simulation model was validated with experimental results for the pure CNG SI engine with main specifications summarized in Table 2. Spark timing was 25 obTDC, λ_{mean} was 1.25 and mean total EGR mass fraction was assumed to be 2%. Figure 6 illustrates the experimental and simulated cylinder pressure variation with crank angle. As seen, there is a good agreement between simulation and experiment.

Figure 7 shows the values of brake torque and BMEP versus engine speed. Simulation results have good agreement with those of experiments within less than 4% deviation. Trend lines of all data are the same. Torque variation as a function of engine speed reflects the variation of volumetric efficiency with engine speed. Falling off in volumetric, mechanical and thermal efficiencies causes the decrease of the brake torque at high engine speed. Torque back-up as its best description was 13% according to the definition [45]:

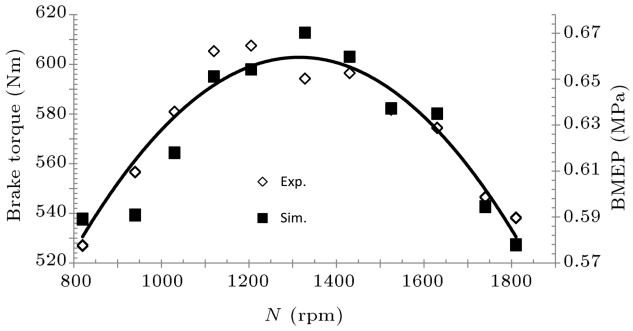

Figure 7. Variation of experimental and simulated values of torque and BMEP with engine speed at $\lambda_{mean} = 1.25$, spark timing of 25°bTDC and WOT.

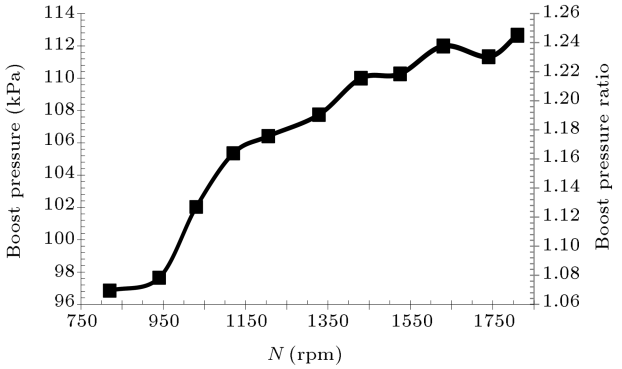

Figure 8. Variation of experimental boost static pressure and its ratio with engine speed at $\lambda_{mean} = 1.25$, spark timing of 25° bTDC and WOT.

$$\text{Torque back-up} = \frac{\text{maximum torque} - \text{torque at maximum speed}}{\text{torque at maximum speed}}. \quad (18)$$

Figure 7 also illustrates variation of experimental and simulated values of BMEP of the engine versus engine speed which is similar to torque variation.

The waste-gated turbocharger has influences on brake torque and its back-up by boost pressure as shown in Figure 8. This Figure shows variation of boost pressure and its ratio versus engine speed. Boost pressure increased linearly up to 1200 rpm, and then its slope decreased. This was due to gradually opening of waste-gate from 1200 to 1450 rpm. Boost pressure became nearly constant at speeds higher than 1450 rpm, as waste-gate opening became nearly constant. By waste-gate opening, torque slope decreased due to lower boost pressure slope as shown in Figure 7. Opening range of waste gate had substantial effects on boost pressure. Figure 8 also shows boost pressure ratio variation with engine speed. It became nearly constant at 1.2 at high speeds.

Figure 9 presents the experimental and simulated values of brake power at different engine speeds. There was a gradual increase in power at high speeds. This

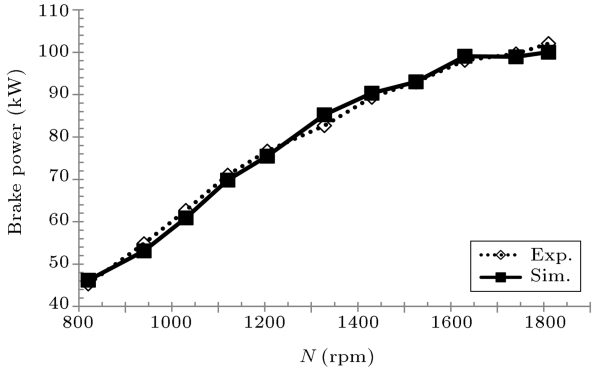

Figure 9. Variation of experimental and simulated values of power with engine speed at $\lambda_{\text{mean}} = 1.25$, spark timing of 25° bTDC and WOT.

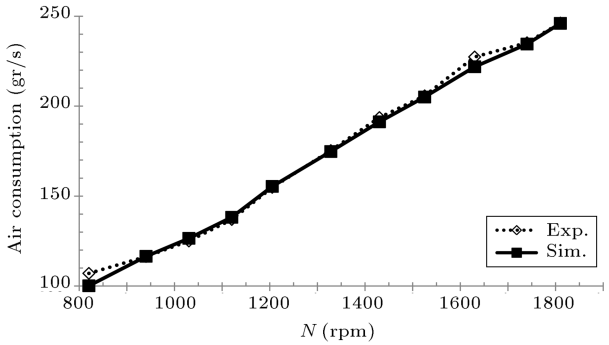

Figure 10. Variation of experimental and simulated values of air consumption with engine speed at $\lambda_{\text{mean}} = 1.25$, spark timing of 25° bTDC and WOT.

trend can be conveniently justified by the volumetric, thermal and mechanical efficiency reductions as engine speed increase. As it can be seen, the simulation result had good agreement with that of experiment.

Figure 10 compares variation of simulated air consumption values versus engine speed with experimental results. As seen, there is a good agreement between simulation and experiment.

Figure 11 shows variation of Brake Specific Fuel Consumption (BSFC) values with engine speed. The simulation result has good agreement with that of experiment within at most 9% deviation. It shows that BSFC first decreases with increase in engine speed up to 1000-1100 rpm and then increases as speed increases further. Higher ratio of heat loss to inlet fuel energy at lower speeds and increase in friction losses including pumping losses at higher speeds were the causes of such variation.

Figure 12 compares variation of simulated air consumption values versus engine speed with experimental results. As can be seen, there is a good agreement between simulation and experiment.

4.2. Parametric studies

The validated code has been used to study the effects of excess air ratio (λ) and spark timing on NO emissions

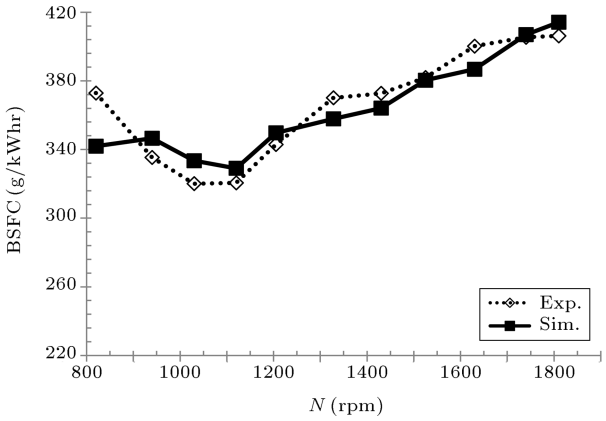

Figure 11. Variation of experimental and simulated values of Brake Specific Fuel Consumption (BSFC) with engine speed at $\lambda_{\text{mean}} = 1.25$, spark timing of 25° bTDC and WOT.

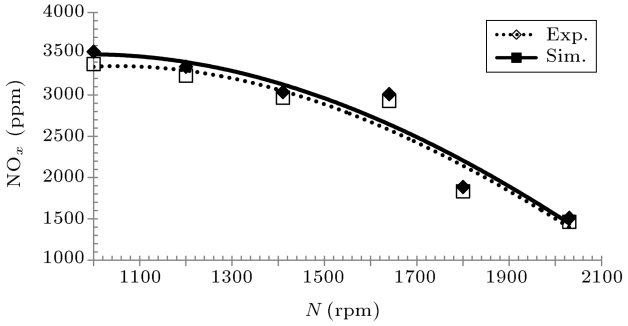

Figure 12. Variation of experimental and simulated values of NO emission with engine speed at $\lambda_{\text{mean}} = 1.2$, spark timing of 25° bTDC and WOT.

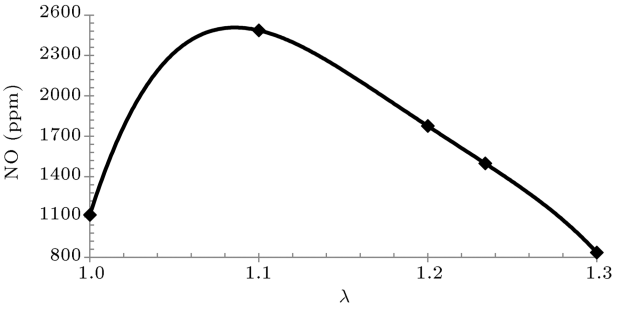

Figure 13. Variation of simulated NO emissions with excess air ratio at 2030 rpm, spark timing of 25° bTDC and WOT.

and also the effects of excess air ratio (λ), EGR and boost pressure on BSFC.

4.2.1. NO emissions

Figure 13 shows the effects of lean-burn on engine NO at 2030 rpm, WOT and spark timing of 25° bTDC. NO emission increased with the increase of excess air ratio until it reached to its peak value at about 1.1 from stoichiometric mixture. The reason is that NO formation mechanism depends on both temper-

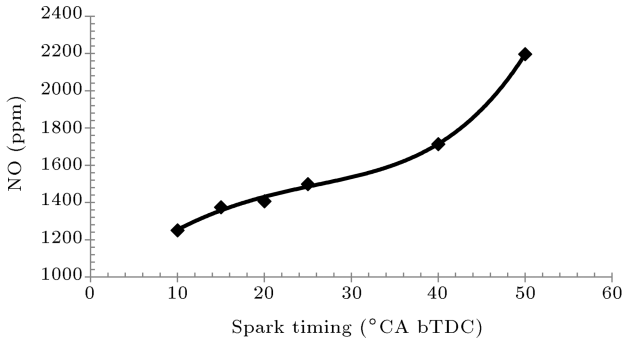

Figure 14. Variation of simulated NO emissions with spark timing at 2030 rpm, $\lambda = 1.234$ and WOT.

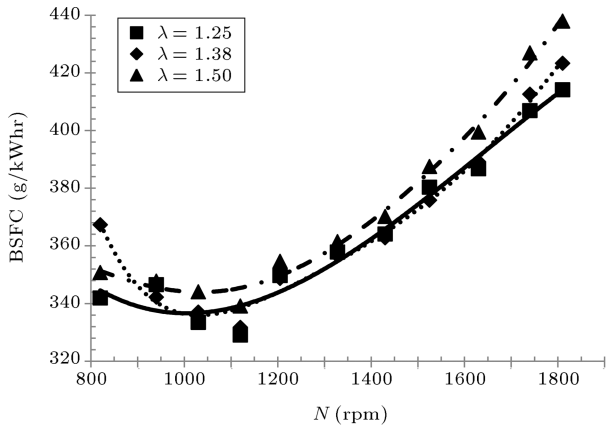

Figure 15. Variation of Brake Specific Fuel Consumption (BSFC) with engine speed at three different excess air ratios at spark timing of 25°bTDC and WOT.

ature and oxygen concentration. Although burned gas temperature is higher for stoichiometric mixture, the availability of oxygen results in the maximum NO emission to be occurred at mixtures slightly leaner than stoichiometric. The burned gas temperature and consequently NO emission decreased when excess air ratio was increased above 1.1.

Figure 14 indicates the effects of spark timing on engine NO at 2030 rpm, WOT and excess air ratio of 1.234. NO emission decreased with increase of spark timing retard. This is due to burned gas temperature reduction as a result of combustion process shift to expansion process. At temperatures lower than 1800 K, the extended Zeldovich mechanism is of low importance due to high activation energy of (1) for detachment of N atom from N_2 molecule with the triple bond.

4.2.2. Excess air ratio

Figure 15 gives effect of increase of excess air ratio on variation of Brake Specific Fuel Consumption (BSFC) with engine speed. Both minimum and average of BSFC increased at a rate of 1% for excess air ratios of 1.38 and 3% for excess air ratios of 1.5 compared with excess air ratios of 1.25. Although the temperature of the burned gas decreased with the increase of excess air

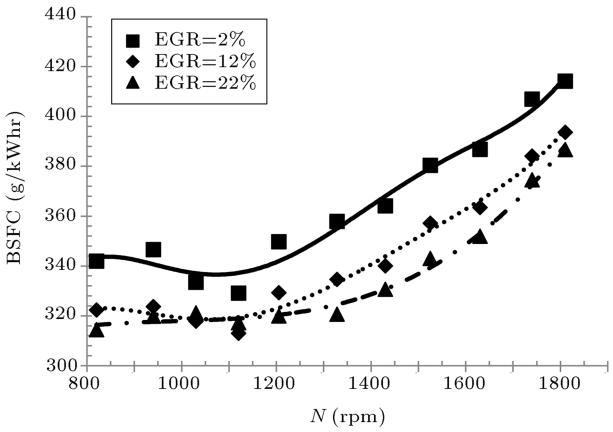

Figure 16. Variation of Brake Specific Fuel Consumption (BSFC) with engine speed at three different EGR mass fractions at $\lambda_{mean} = 1.25$, spark timing of 25°bTDC and WOT.

ratio, combustion duration increased substantially and led to a little increase in BSFC. At higher excess air ratios, flame speed decreased and created drivability problems and at most partial burning of the charge. Another effect of lean operation is the lower exhaust gas temperature which is of high importance for the efficiency of the catalyst, if it exists. Engine durability and cost improve with the increase of excess air ratio.

4.2.3. Exhaust Gas Recirculation (EGR)

Figure 16 indicates effects of three EGR mass fractions on variation of BSFC with engine speed. Increase of EGR at a rate of 20% reduced the minimum and average of BSFC, 5% and 8%, respectively. EGR containing CO_2, H_2O and N_2 caused higher overall heat capacity of the in-cylinder mixture in comparison with O_2 and N_2 which are normally a part of inlet air. It resulted in lower burned gas temperature. CO_2, H_2O and N_2 also dissociated at high flame temperatures and reduced burned gas temperature more. Lower burned gas temperature resulted in lower heat loss importance to cylinder walls and improved BSFC. The effect of lower burned gas temperature was higher than longer combustion duration due to lower O_2 concentration that shifts combustion to expansion process. Higher EGR also improves engine mechanical efficiency; therefore BSFC decreases as EGR increases.

4.2.4. Boost pressure ratio

Figure 17 illustrates BSFC variations at three curves of increase in the boost pressure ratio, which have similar trend with Figure 8. Here, by increasing the boost pressure ratio up to 0%, 10% and 20%, maximum boost ratios of 1.24, 1.37 and 1.49 are obtained, respectively. The boost pressure ratio increase caused BSFC decrease, because engine friction depends on speed and not on boost pressure considerably. Therefore higher charge mixture at higher boost ratio produces higher

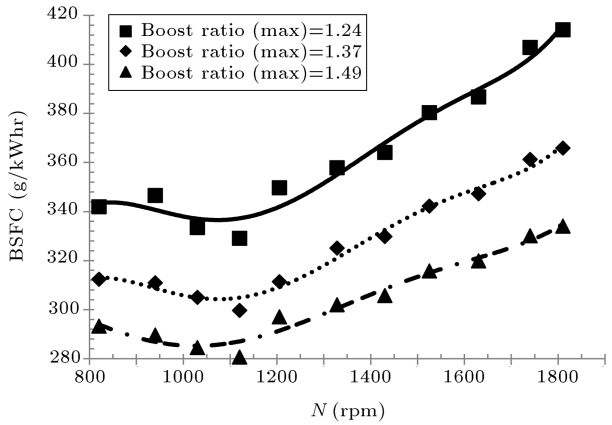

Figure 17. Variation of Brake Specific Fuel Consumption (BSFC) with engine speed at three different boost pressure ratios at $\lambda_{\text{mean}} = 1.25$, spark timing of 25°bTDC and WOT.

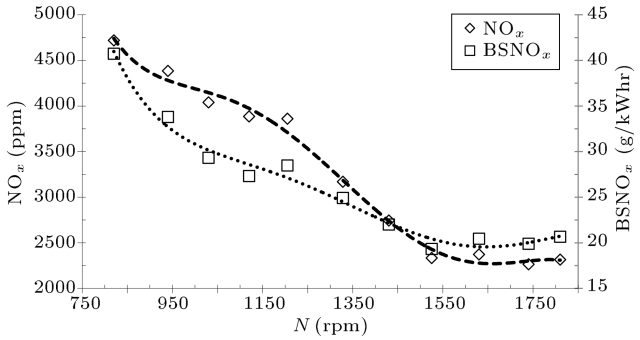

Figure 18. Variation of experimental NO_x and $BSNO_x$ with engine speed at $\lambda_{\text{mean}} = 1.25$ and WOT.

brake power per 1 g fuel considering nearly constant engine friction with boost pressure change.

4.3. NO_x emission

Figure 18 illustrates variation of NO_x emission in exhaust gases with engine speed at $\lambda_{\text{mean}} = 1.25$ and WOT. NO_x emission occurs in hot combustion products. Three main factors which cause NO_x emission, are oxygen availability, high temperatures (more than 1800 K) and the time duration that combustion products remain at high temperature [26]. Enough oxygen was available in the combustion process at the present lean running conditions. The spark timing was kept constant over the speed range. Therefore, comparing with MBT timing, spark timing was relatively retard at high engine speeds, causing a lower NO_x emission due to shifting combustion process to expansion stroke with lower flame and combustion product temperatures. CNG fuel like other gaseous fuels does not have the cooling effect of vaporization. Therefore, the mixture temperature at IVC would be high. The time duration of high combustion temperature decreases as the engine speed increases. Also flow pressure drop of gas exchange processes was bigger at higher engine

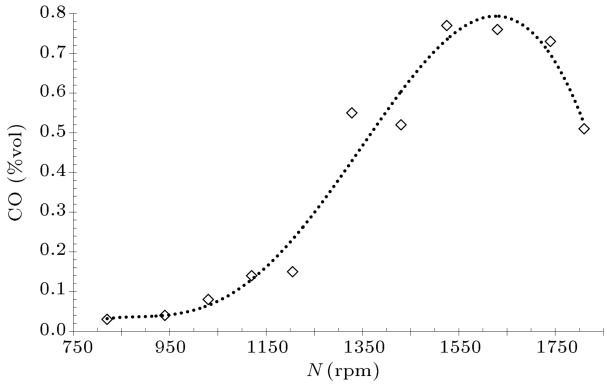

Figure 19. Variation of experimental CO concentration with engine speed at $\lambda_{\text{mean}} = 1.25$ and WOT.

speeds during valve overlap, consequently, residual gas fraction increased and led to decrease in NO_x emission at higher engine speed.

Figure 18 also shows variation of brake specific NO_x emission in exhaust gases with engine speed at $\lambda_{\text{mean}} = 1.25$ and WOT. Specific emission (g/kWh) is derived from emission concentration by:

Brake specific emission

$$= 3600 \frac{\text{MW}_{\text{emission}}}{\text{MW}_f} \frac{\dot{m}_f}{P_b} N_{\text{mix,dry}} \chi_{\text{emission}}, \tag{19}$$

where $\dot{m}_f$ is fuel consumption mass flow rate in g/s, χ_{emission} emission volumetric concentration, MW_f and $\text{MW}_{\text{emission}}$ are molecular weight of fuel and emission, respectively, in g/mole, P_b is brake power in kW and $N_{\text{mix,dry}}$ is the total mole number of products per mole of fuel C_xH_y for dry concentrations according to [46]:

$$N_{\text{mix,dry}} = 4.773 \left[\frac{x + (1 - \chi_{O_2,\text{dry}}) y/4}{1 - 4.773 \chi_{O_2,\text{dry}}} \right] - y/4, \tag{20}$$

in which $\chi_{O_2,\text{dry}}$ is the concentration of dry oxygen in exhaust gases.

The $BSNO_x$ reduced with the increase of engine speed due to spark retard (comparing with MBT timing), smaller duration of high combustion temperatures and lower residual gas (or internal EGR), as explained for NO_x concentration.

4.4. CO emission

Figure 19 illustrates CO emission concentration in the engine exhaust gases. Poor mixing of air and fuel, incomplete combustion and rich regions produce higher concentration of CO. It also substantially depends on excess air ratio. At the lean mixture conditions, CO in exhaust gases was due to poor mixing and incomplete combustion. At constant spark timing during all speed range, combustion shifted to expansion stroke as speed increased and caused lower combustion temperature and higher CO emission.

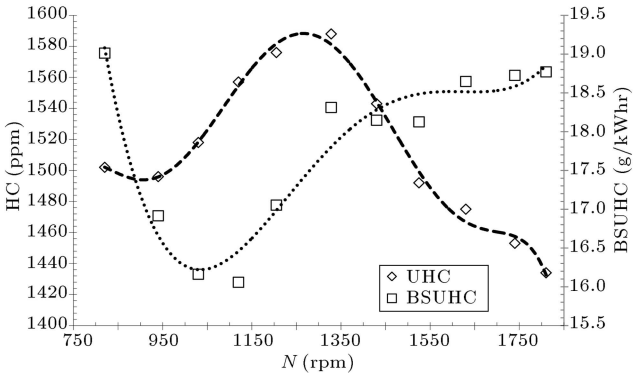

Figure 20. Variation of experimental UHC and BSUHC with engine speed at $\lambda_{\text{mean}} = 1.25$ and WOT.

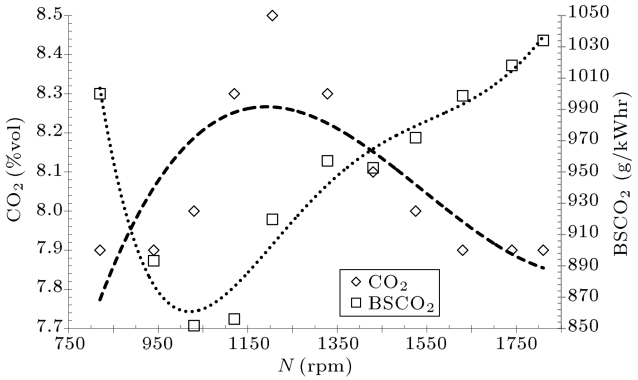

Figure 21. Variation of experimental CO_2 and $BSCO_2$ with engine speed at $\lambda_{\text{mean}} = 1.25$ and WOT.

4.5. Exhaust unburned hydrocarbon

Figure 20 shows variation of unburned hydrocarbon and BSUHC in exhaust emission with engine speed at $\lambda_{\text{mean}} = 1.25$ and WOT. Flame quenching near wall surfaces and flame extinguishment within crevices, as well as excessive cooling of the flame front, are sources of HC development in engines at lean and especially rich conditions. The trend was compatible with expectations.

Figure 20 also indicates a minimum value of 16 g/kWh for BSUHC at 1120 rpm. As seen from Figure 11, the point of best BSFC was at speeds around 1000-1100 rpm which corresponds to minimum BSFC. This region obviously had the optimum combustion and operation conditions and should provide the minimum BSHC.

4.6. CO_2 emission

Figure 21 shows variation of exhaust gas brake specific CO_2 and $BSCO_2$ with engine speed at $\lambda_{\text{mean}} = 1.25$ and WOT. $BSCO_2$ had a minimum value of 852 g/kWh at 1030 rpm with an average value of 2.6 g CO_2/g NG for the test. The point of minimum $BSCO_2$ corresponded to the point of minimum BSFC and optimum operating conditions as seen in Figure 11.

Figure 21 also illustrates variation of CO_2 in exhaust gases with engine speed. CO_2 reduced at high engine speed and attained a maximum in the medium speed range.

5. Conclusions

In this paper, a turbocharged natural gas SI engine was experimentally investigated at lean operating conditions. A model was also developed and validated with experimental performance results. Good agreement between simulated and experimental results showed the accuracy of the developed model. Effects of excess air ratio, EGR and boost pressure on BSFC as well as effects of the excess air ratio and spark timing on NO emissions were investigated by parametric study. Experimental emission and performance characteristics of the engine were studied and discussed. The main results are summarized as follows:

1. As a novel approach, it has been assumed that thermal boundary layer thickness is equal to quench layer thickness. The thickness should be equal to a value if be subtracted from cylinder dimensions, total mass fraction burned is equal to corresponding experimental value. This assumption provides good agreement between simulated and experimental mass fraction burned curves.
2. Considering a thermal boundary layer in simulation has substantial importance in mass fraction burned curve, although its effect on cylinder pressure simulation is low.
3. Waste-gated turbocharger affects the brake torque. By waste-gate opening, torque slope decreases due to lower boost pressure slope. Torque decreases with further opening of waste-gate as engine speed increases. This results in a better torque back-up.
4. The BSFC is min at medium engine speeds due to a lower heat and friction losses at WOT.
5. NO emission increases with the increase of excess air ratio until it reaches its peak value at about 1.1 from stoichiometric mixture and then decreases. NO emission also decreases with increase of spark timing retard substantially.
6. The use of higher excess air ratio at a rate of 20% increases minimum of BSFC 3% at constant design and operating parameters.
7. It was found that increase of EGR at a rate of 20% improves minimum of BSFC 5%.
8. Gradual opening of waste-gate decreases boost pressure gradient as speed increases at WOT. Then boost pressure remains nearly constant at speeds higher than 1450 rpm.
9. The $BSNO_x$ reduces with engine speed increase. It is due to the spark retard compared to MBT timing,

shorter time for high combustion temperatures and higher residual gas mass fraction.

10. The trend of $BSCO_2$ versus engine speed is similar to the BSFC, as expected.

Acknowledgements

The authors acknowledge research assistants for their engineering support and also lab staff for their cooperation at the lab. Research vice-presidency of Sharif University of Technology is also acknowledged for their financial support.

Nomenclature

k	Turbulent kinetic energy
l_i	Turbulence integral length scale
MW	Molecular Weight
N	Engine speed (rpm)
NO_x	Nitric oxides
$N_{mix,dry}$	Total mole number of products per mole of fuel
P	Pressure (kPa)
P_b	Brake power (kW)
p_{cyl}	Cylinder pressure (bar)
$\dot{q}_{ac}$	Engine air consumption
Re_T	Turbulent Reynolds number
rg_{Vol}	Residual gas volumetric fraction
rpm	Round per minute
S_L	Laminar flame speed
S_T	Turbulent flame speed
T_u	Unburned mixture temperature
T	Temperature (K)
u'	Turbulence intensity
λ_{mean}	Mean excess air ratio
μ	Unburned mixture dynamic viscosity
ρ	Air density
ρ_U	Unburned mixture density
ρ_s	Air density at standard conditions
σ	Air density to its standard density ($=\rho/\rho_s$)
Φ	Fuel air equivalence ratio
$\chi_{emisson}$	Emission volumetric (or molar) emission
$\chi_{O_2,dry}$	O_2 dry concentration in exhaust gases
ΔP	Pressure difference (mmHg and mmH_2O)

Acronyms

BMEP	Brake Mean Effective Pressure
$BSCO_2$	Brake Specific CO_2 emission
BSFC	Brake Specific Fuel Consumption
$BSNO_x$	Brake Specific NO_x emission
BSUHC	Brake specific unburned hydrocarbon
bTDC	Before Top Dead Center
CA	Crank Angle
CI	Compression Ignition
CNG	Compressed Natural Gas
ECE	Economic Commission for Europe
EGR	Exhaust Gas Recirculation
EXP	Experimental
GHG	Green House Gas
IMEP	Indicated Mean Effective Pressure
IVC	Intake Valve Close
MBT	Minimum advance for Best Torque
RON	Research Octane No.
SI	Spark Ignition
SIM	Simulated
TBL	Thermal Boundary Layer
TDC	Top Dead Center
TKE	Turbulent Kinetic Energy
UHC	Unburned hydrocarbon
WOT	Wide Open Throttle

Subscripts

b	Burned
cyl.	Cylinder
f	Fuel
L	Laminar
T	Turbulent
u	Unburned

References

1. Korakianitis, T., Namasivayam, A.M. and Crookes, R.J. "Natural-gas fueled spark-ignition (SI) and compression-ignition (CI) engine performance and emissions", *Progress in Energy and Combustion Science*, **37**, pp. 89-112 (2011).

2. Cho, H.M. and He, B. "Spark ignition natural gas engines - A review", *Energy Conversion and Management*, **48**, pp. 608-618 (2007).

3. Kharazmi, Sh., Mozafari, A. and Hajilouy-Benisi, A. "Simulating turbulence and combustion in CNG turbocharged engine considering cylinder thermal bound-

ary layer and EGR", *Proceedings of the Seventh International Conference on Internal Combustion Engines*, Olympic Hotel, Tehran, Iran (November 8-10, 2011).

4. Kandarp, Bhatt K. "Potential for meeting the EU new passenger car CO_2 emissions target", M.Sc. Thesis, MIT University (2010).

5. Ibrahim, A. and Bari, S. "An experimental investigation on the use of EGR in a supercharged natural gas SI engine", *Fuel*, **89**, pp. 1721-1730 (2009).

6. Rothlisberger, R.P. and Favrat, D. "Comparison between direct and indirect (prechamber) spark ignition in the case of a cogeneration natural gas engine, part I: engine geometrical parameters", *Applied Thermal Engineering*, **22**, pp. 1217-1229 (2002).

7. Rothlisberger, R.P. and Favrat, D. "Comparison between direct and indirect (prechamber) spark ignition in the case of a cogeneration natural gas engine, part II: Engine operating parameters and turbocharger characteristics", *Applied Thermal Engineering*, **22**, pp. 1231-1243 (2002).

8. Kharazmi, Sh., Hajilouy-Benisi, A. and Mozafari, A. "Computer simulation of turbocharged aftercooled gasoline engine", *Proceedings of ESDA2006, 8th Biennial ASME Conference on Engineering Systems Design and Analysis*, Torino, Italy (July 4-7, 2006).

9. Gharehghani, A., Koochak, M., Mirsalim, M. and Yusaf, T. "Experimental investigation of thermal balance of a turbocharged SI engine operating on natural gas", *Applied Thermal Engineering*, **60**(1-2), pp. 200-207 (2013).

10. Park, C., Kim, C. and Choi, Y. "Power output characteristics of hydrogen-natural gas blend fuel engine at different compression ratios", *International Journal of Hydrogen Energy*, **37**, pp. 8681-8687 (2012).

11. Ibrahim, A. and Bari, S. "A comparison between EGR and lean-burn strategies employed in a natural gas SI engine using a two-zone combustion model", *Energy Conversion and Management*, **50**, pp. 3129-3139 (2010).

12. Kesgin, U. "Study on prediction of the effects of design and operating parameters on NO_x emissions from a lean burn natural gas engine", *Energy Conversion and Management*, **44**, pp. 907-921 (2003).

13. Kesgin, U. "Genetic algorithm and artificial neural network for engine optimization of efficiency and NO_x emission", *Fuel*, **83**, pp. 885-895 (2004).

14. Kesgin, U. "Effect of turbocharging system on the performance of a natural gas engine", *Energy Conversion and Management*, **46**, pp. 11-32 (2005).

15. Kesgin, U. "Study on design of inlet and exhaust system of a stationary internal combustion engine", *Energy Conversion and Management*, **46**, pp. 2258-2287 (2005).

16. Pourkhesalian, A.M., Shamekhi, A.H. and Salimi, F. "Alternative fuel and gasoline in an SI engine: A comparative study of performance and emissions characteristics", *Fuel*, **89**, pp. 1056-1063 (2010).

17. Lammle, C. "Numerical and experimental study of flame propagation and knock in a compressed natural gas engine", PhD Thesis, Swiss Federal Institute of Technology ETH, Zurich, Switzerland (2005).

18. Gulder, O.L. "Turbulent premixed flame propagation models for different combustion regimes", *23rd Symposium (International) on Combustion*, pp. 743-750 (1990).

19. *NIST-JANAF Thermochemical Tables*, published by American Chemical Society and American Institute of Physics for National Institute of science and Technology, 4th Ed. (1998).

20. Kharazmi, Sh., Hajilouy-Benisi, A. and Mozafari, A., "Experimental investigation of waste gate effects on CNG turbocharged SI engine and its turbocharger", *Proceedings of the 20th Annual International Iranian Mechanical Engineering Conference*, Shiraz University, Shiraz, Iran (in Persian, Presented Orally) (May 16-18, 2012).

21. Martyr, A.J. and Plint, M.A., *Engine Testing Theory and Practice*, Elsevier ltd, 3rd Edn. (2007).

22. Garret Airesearch Industrial Division (AID), *Flow Measurement with AID Flow Nozzles* (1975).

23. AVL, *Operational Manual, Engine Diagnostics*, AVL DiCom 4000, AVL (2001).

24. Hohenberg, G.F. "Advanced approaches for heat transfer calculations", SAE International, S.A.E. Paper. No. 790825, in SP- 449 (1979).

25. Watson, N. and Janota, M.S., *Turbocharging the Internal Combustion Engine*, MACMILLAN PRESS LTD (1982).

26. Heywood, J.B., *Internal Combustion Engine Fundamentals*, New York, McGraw-Hill Book Company (1988).

27. Shy, S.S., Chen, Y.C., Yang, C.H., Liu, C.C. and Huang, C.M. "Effects of H_2 or CO_2 addition, equivalence ratio, and turbulent straining on turbulent burning velocities for lean premixed methane combustion", *Combustion and Flame*, **153**, pp. 510-524 (2008).

28. Yoshida, A., Naito, H. and Mishra, D.P. "Turbulent combustion of preheated natural gas-air mixtures", *Fuel*, **87**, pp. 605-611 (2008).

29. Bromberg, L. "In-cylinder laminar flame propagation speed: effects of hydrogen and hydrogen rich gas addition", *MIT Plasma Science and Fusion Center*, (August 25, 2005).

30. "Laminar flame speed of stoichiometric methane/air premixed flame", Application note of CHEMKIN-PRO, Pro-APP-AUTO-3 (v1.0) (May 14, 2008).

31. Ji, M., Miao, H., Jiao, Q., Huang, Q. and Huang, Z. "Flame propagation speed of CO_2 diluted hydrogen-enriched natural gas and air mixtures", *Energy Fuels*, **23**, pp. 4957-4965.

32. Rozenchan, G., Zhu, D.L., Law, C.K. and TSE, S.D. "Outward propagation, burning velocities and chemical effects of methane flame up to 60 ATM", *Proceeding of the Combustion Institute*, **29**, pp. 1461-1469 (2002).

33. Yu, G., Law, C.K. and Wu, C.K. "Laminar flame speeds of hydrogen + air mixtures with hydrogen addition", *Combustion and Flame*, **63**, pp. 339-347 (1986).

34. Bell, J.B., Day, M.S., Almgren, S., Cheng, R.K. and Shepherd, I.G. "Numerical simulation of premixed turbulent methane", Lawrence Berkeley National Laboratory.

35. Gu, X.J., Haq, M.Z., Lawes M. and Woolley, R. "Laminar burning velocity and Markstein lengths of methane-air mixtures", *Combustion and Flame*, **121**, pp. 41-58 (2000).

36. Liao, S., Jiang, D. and Cheng, Q. "Determination of laminar burning velocities for natural gas", *Fuel*, **83**, pp. 1247-1250 (2004).

37. Elia, M., Ulinski, M. and Metghalchi, M. "Laminar burning velocity of methane-air_diluent mixtures", *Transactions of ASME, Journal of Engineering for Gas Turbines and Power*, **123**, pp. 190-196 (2001).

38. Rahim, F., Elia, M., Ulinski, M. and Metghalchi, M. "Burning velocity measurement of methane-oxygen-argon mixtures and an application to extended methane-air burning velocity measurements", *International Journal of Engine Research*, **3**(2), pp. 81-92 (2002).

39. Gulder, O.L. "Turbulent premixed flame propagation models for different combustion regimes", *23rd Symposium (International) on Combustion*, pp. 743-750 (1990).

40. Verhelst, S., Sheppard, C.G.W. "Multi-zone modeling of spark-ignition engine simulation - An overview", *Energy Conversion and Management*, **50**, pp. 1326-1335 (2009).

41. Keck, J.C. "Turbulent flame structure and speed in spark-ignition engines", *19th Symposium (International) on Combustion/ the Combustion Institude*, pp. 1451-1466 (1982).

42. Lyford-Pike, E.J. and Heywood, J.B. "Thermal boundary layer thickness in the cylinder of a spark ignition engine", *International Journal of Heat Mass Transfer*, **27**(10), pp. 1873-1878 (1984).

43. Smith, G.P., Golden, D.M., Frenklach, M., Moriarty, N.W., Boris Eiteneer, B., Goldenberg, M., Bowman, C.T., Hanson, R.K., Song, S., Gardiner, W.C. Jr., Lissianski, V.V. and Qin, Zh., Gas Research Institute, http://www.me.berkeley.edu/gri_mech/

44. Lounici, M.S., Loubar, Kh., Balistrou, M. and Tazerout, M. "Investigation on heat transfer evaluation for a more efficient two-zone combustion model in the case of natural gas SI engines", *Applied Thermal Engineering*, **31**, pp. 319-328 (2011).

45. Atkins, R.D. "An introduction to engine testing and development", *SAE International*, SAE No. R-344 (2009).

46. Turns, S.R., *An Introduction to Combustion: Concepts and Applications*, 2nd En., McGraw Hill (2000).

Biographies

Shahaboddin Kharazmi received his BSc in Mechanical Engineering in 2003 and MSc in Automotive Engineering in 2005 from Sharif University of Technology, Tehran, Iran. He then followed the Mechanical Engineering PhD program at Sharif University of Technology in 2006 as a talented student, without need to entrance exam. Throughout his university and industry career, he has worked with automotive power train system especially internal combustion engine. He is author or co-author of over 10 national and international conference and journal papers. He has worked as a MSc and PhD student in engine research lab and turbocharger & turbocharging lab and developed engine combustion analysis system as well as eddy current dynamometer system at Sharif University of Technology. He has taught Automechanic Workshop and also Heat Transfer, Thermodynamics and Fluid Mechanics Labs as well as being Teacher Assistant in Fluid Mechanics II and Thermodynamics I all in Mechanical Engineering Department. of Sharif University of Technology.

Aliasghar Mozafari received his PhD degree from University of London (Q.M.C.), UK in 1988. He has been a faculty member of Mechanical Engineering Department at Sharif University of Technology (SUT) for 38 years. He has been head of Mechanical Engineering Department for six years and Educational Deputy of Mechanical Engineering Deptartment for four years. He has been member of Center of Excellence in Energy Conversion as well as Director of International Students' Office at SUT. He is author or co-author of over 90 national and international conference and journal papers and has supervised over 40 graduate theses. He has also published a book in 1993.

Ali Hajilouy Benisi received his PhD degree from the Mechanical Engineering Department of Imperial College at the University of London in 1993. He has been faculty member of the Institute of Water and Energy and then the School of Mechanical Engineer-

ing at Sharif University of Technology (SUT) since 1978. He served as Director of the Fluid Mechanics Lab. from 1993-1995, Founder and Director of the Turbocharger Lab. from 1993, Founder and Director of the Turbocharging Lab. from 2000, Founder and Director of the Gas Turbine Lab. from 2008, at the School of Mechanical Engineering of SUT. He has also served as Research Director of the SUT from 1993-1995. His research interests are experimental and theoretical investigations of turbochargers, turbocharging, and gas turbines.

Dr Hjilouy Benisi is author or co-author of over 90 conferences and journal papers, and coordinator for compiling and publishing four volumes research reports of SUT in 1991-1995. He and one of his students are translators of an English text book to Farsi (Persian). He has also supervised over 40 graduate theses. He has conducted more than seven research funded projects.